

# Geophysical Research Letters

## RESEARCH LETTER

10.1029/2019GL083712

### Key Points:

- Superposed epoch analysis around clusters of substorms show consistent radiation belt dynamical responses to mild geomagnetic disturbances
- Magnetopause shadowing produces proton and electron loss over a wide range of  $L$ -shells, eventually modified by substorm flux enhancements
- Twofold increases in daily substorm occurrence during periods of sudden particle enhancements at low  $L$  shells suggests a common linkage

### Correspondence to:

C. J. Rodger,  
crodger@physics.otago.ac.nz

### Citation:

Rodger, C. J., Turner, D. L., Clilverd, M. A., & Hendry, A. T. (2019). Magnetic local time-resolved examination of radiation belt dynamics during high-speed solar wind speed-triggered substorm clusters. *Geophysical Research Letters*, 46. <https://doi.org/10.1029/2019GL083712>

Received 14 MAY 2019

Accepted 26 AUG 2019

Accepted article online 29 AUG 2019

## Magnetic Local Time-Resolved Examination of Radiation Belt Dynamics during High-Speed Solar Wind Speed-Triggered Substorm Clusters

Craig J. Rodger<sup>1</sup> , Drew L. Turner<sup>2</sup> , Mark A. Clilverd<sup>3</sup> , and Aaron T. Hendry<sup>4</sup> 

<sup>1</sup>Department of Physics, University of Otago, Dunedin, New Zealand, <sup>2</sup>Space Sciences Department, Aerospace Corporation, El Segundo, CA, USA, <sup>3</sup>British Antarctic Survey (NERC), Cambridge, UK, <sup>4</sup>Department of Space Physics, Institute of Atmospheric Physics, Prague, Czechia

**Abstract** Particle observations from low Earth orbiting satellites are used to undertake superposed epoch analysis around clusters of substorms, in order to investigate radiation belt dynamical responses to mild geomagnetic disturbances. Medium energy electrons and protons have drift periods long enough to discriminate between processes occurring at different magnetic local time, such as magnetopause shadowing, plasma wave activity, and substorm injections. Analysis shows that magnetopause shadowing produces clear loss in proton and electron populations over a wide range of  $L$ -shells, initially on the dayside, which interacts with nightside substorm-generated flux enhancements following charge-dependent drift directions. Inner magnetospheric injections recently identified as an important source of tens to hundreds keV electrons at low  $L$  ( $L < 3$ ), occurring during similar solar wind-driving conditions as recurrent substorms, show similar but more enhanced geomagnetic AU-index signatures. Twofold increases in substorm occurrence at the time of the sudden particle enhancements at low  $L$  shells (SPELLS) suggest a common linkage.

**Plain English Summary** The magnetic field of the Earth is filled with high-energy particles, primarily electrons and protons, forming the Van Allen radiation belts. Over the years it has become obvious that the number of trapped high-energy electrons changes rapidly, and in complex ways. We know that multiple different processes are involved to produce such dynamic changes, which include energization, transport, and loss. Over the last ~7 years flagship science missions have been launched by multiple space agencies to better understand the complex dynamics. However, these involve only 1 or 2 highly instrumented spacecraft—these make extremely high-quality measurements but are limited by their inability to be in multiple places at the same time. Nonetheless, signatures of several different processes have been identified and described. In the current study we use a constellation of spacecraft with more limited instrumentation than the flagship missions. This has allowed us to clarify the typical dynamical processes affecting radiation belt particles. In particular, the ability to measure simultaneously at multiple locations, plus statistical averaging, allows us to show clear evidence of the loss process termed magnetopause shadowing. We also cast light on a previously mysterious process of sudden particle enhancements occurring deep in the belts.

## 1. Introduction

The temporal evolution of radiation belt electron fluxes is highly dynamic, particularly for the outer radiation belt. Multiple different processes have been identified, which can drive electron energization (often termed acceleration), loss, or transport (see, e.g., Balasis et al., 2016; Baker et al., 2018). Typically, the occurrence and magnitude of these processes are dependent upon distance from the Earth (expressed, e.g., through the  $L$ -shell), particularly due to the changing cold plasma density and the strong gradients around the plasmopause. At the same time, the processes also depend very strongly on magnetic local time (MLT). The trapped radiation belt electron flux at a given point in space at a given time depends on a combination of multiple processes—in order to understand the evolution of trapped flux it is necessary to understand the MLT-dependent dynamical processes in some detail. Typically, MLT dependence is averaged over processes that take significantly longer than the electron drift period, and as such have not been clearly seen in many experimental studies.

There are multiple examples of  $L$  and MLT-dependent activity influencing radiation belt electron flux evolution on timescales faster than the electron drift period. One is magnetopause shadowing on the dayside (e.g., Turner et al., 2012; Yu et al., 2013) where electrons drifting around the Earth encounter the magnetopause and are lost into the solar wind. Another is the strong MLT variation seen in plasma wave activity (e.g., Figure 7 of Summers et al., 1998), which is likely responsible for the  $L$  and MLT variation seen in precipitation into the atmosphere (e.g., Carson et al., 2012; Douma et al., 2017; van de Kamp et al., 2018). A third example is magnetospheric substorms, short-lived reconfigurations of the geomagnetic field where energetic particles are injected into the inner magnetosphere close to magnetic midnight (Akasofu, 1981; Cresswell-Moorcock et al., 2013).

In many cases we have a good physical understanding of how the  $L$  and MLT-dependent activity will drive changes in radiation belt fluxes; however, it is not always easy to observe these dynamical changes occurring in situ and discriminate between the actions of individual processes. One strong reason for this is the rapid drift time of relativistic electrons. The drift period of a trapped 1-MeV electron at  $L=5$  is  $\sim 13.5$  min (calculated through expressions in Walt, 1994). Even a dramatic change occurring in one MLT region will rapidly drift through all other sectors making it hard to determine where it originated from; such rapid drift rates compared to the time resolution of the analysis also mean MLT-dependent impacts are rapidly “smeared” around the Earth, especially considering spacecraft revisit periods of  $\sim 1$  hr to a day, or more. In contrast, the drift period of a trapped 150-keV electron at  $L=5$  is almost 70 min. In the current study we use electrons with energies of hundreds of keV, which drift much more slowly than MeV electrons, and hence, individual processes can be distinguished using a network of low Earth orbit (LEO) satellites with  $\sim 100$ -min orbital periods.

In the last decade or so, our understanding of the radiation belts has markedly increased, in large part due to flagship space missions (examples being the Van Allen Probes and Arase), along with the concentrated scientific attention such large-scale activity attracts. However, the cost of such high-quality scientific platforms limits the number which will operate at any given time. In recent years there has been a wealth of exceptional in situ observations deepening our understanding (e.g., Aseev et al., 2017; Jaynes et al., 2015; Kasahara et al., 2018; Turner et al., 2019; Xiang et al., 2018; Zhao et al., 2017) but which are limited in their ability to provide simultaneous MLT and  $L$  coverage.

This is an area in which spacecraft with more limited instrumentation in LEO can assist, as they already exist as constellations of multiple satellites simultaneously monitoring different MLTs while rapidly moving through  $L$ -shells. In this study we make use of observations from a constellation of polar-orbiting LEO satellites, which have employed the same experimental equipment to make measurements of medium energy electrons in the radiation belts for  $>15$  years. Using these observations as a “big data” set, we undertake superposed epoch analysis (SEA) around clusters of substorms, inner magnetospheric activity expected to produce a strong radiation belt dynamical response (Jaynes et al., 2015; Miyoshi et al., 2013; Rodger et al., 2016). The analysis demonstrates the high level of dynamical variation in radiation belt structure with MLT. By focusing on medium energy electrons we can discriminate between processes occurring at different MLT.

## 2. Experimental Datasets

### 2.1. POES SEM-2 Particle Observations

The Polar Orbiting Environmental Satellites (POES) are a set of LEO spacecraft ( $\sim 800$ – $850$  km) in  $\sim 100$ -min period Sun-synchronous polar orbits. Since NOAA-15 in 1998, this series of spacecraft have monitored medium energy electron and proton fluxes with the Medium Energy Proton and Electron Detector (Evans & Greer, 2004; Rodger, Carson, et al., 2010; Rodger, Clilverd, et al., 2010) as part of the Space Environment Monitor (SEM-2) package (Evans & Greer, 2004). Here we focus on the trapped electron and proton flux observations from the 90-degree telescopes, which are named 90eX and 90PX, where X is the channel number (see Evans & Greer, 2004, and Rodger, Clilverd, et al., 2010, for more details). We restrict ourselves to the 90-degree telescope observations as these primarily measure trapped particles (Rodger, Carson, et al., 2010; Rodger, Clilverd, et al., 2010), the dynamics of which are the focus of the current study.

During the period analyzed in our study (2005–2013), an increasing number of POES spacecraft were launched, including the U.S. NOAA-15 through to NOAA-19 and the European MetOp-1 and 2. Due to

the large number of POES spacecraft, and their LEO orbits, there is very good coverage across  $L$  and MLT (e.g., Hendry et al., Fig. 1, 2016). We have combined the observations from multiple satellites into an  $L$  and time grid of median flux values with a 0.25  $L$ -resolution and a 15-min time resolution. This is undertaken for a series of MLT range: 0–3, 3–6, 6–9, through to 21–24 MLT. A more detailed description of the dataset and the processing undertaken can be found in Rodger, Clilverd, et al. (2010) and Cresswell-Moorcock et al. (2013).

## 2.2. Recurrent Substorm Epochs

As noted above, we will undertake SEA on “clusters” of substorms and make use of the substorm lists produced by SuperMAG (Gjerloev, 2012; Newell & Gjerloev, 2011a). We follow the definition of Newell and Gjerloev (2011b) and their naming convention of “recurrent” substorm groupings, the definition of which is described below. For the current study the SuperMAG substorm list was generated on 25 August 2014, 18:57:19 UT. This is the same “recurrent” substorm list used in Rodger et al. (2016), spanning 2005–2013. We make use of this listing as its properties, links to solar wind and geomagnetic activity, and non-MLT dependent radiation belt SEA were described in detail in Rodger et al. (2016). This allows us to focus in this research letter specifically on the MLT dependent behavior of the same set of events.

The epoch event time is taken as the time of the first substorm in a cluster of 2 or more substorms, which are closely spaced in time, using the clustering definition of Newell, Gjerloev (2011b). The start of the cluster must have >82 min between it and any previous events. Each subsequent substorm in the chain must be spaced  $\leq 82$  min after its immediate previous neighbor. There is no restriction on the length of the recurrent substorm chain. Following Rodger et al. (2016), there are 2,052 unique recurrent substorm epochs.

## 3. MLT-Resolved Dynamical processes

### 3.1. Overview

Rodger et al. (2016) showed that the recurrent substorm epochs begin during times of high solar wind speeds when the interplanetary magnetic field [IMF]  $B_z$  turns southward. Following the recurrent substorm epochs there are enhancements in lower band whistler mode chorus and energetic electron fluxes in the radiation belts. It is important to note that both the chorus and flux enhancements start before the zero epoch, consistent with acceleration driven by enhanced magnetospheric convection driven by large-amplitude Alfvén waves in the solar wind (Lyons et al., 2005). However, there is a much stronger whistler mode chorus enhancement after the zero epoch (Rodger et al., 2016), consistent with the importance of substorms providing a population of chorus-producing source electrons (e.g., Jaynes et al., 2015; Simms et al., 2018).

Unremarked in the text of the Rodger et al. (2016) study is the clear increase (shown in the right-hand side of Figure 4 of that study) for inner belt and slot region >100-keV electrons occurring after the recurrent substorm zero epoch. We argue that this is consistent with what has recently been named sudden particle enhancements at low  $L$ -shells (SPELLS) (Turner et al., 2017). The SPELLS reports stimulated the research efforts detailed in this current work.

It is important to note that the epochs used here are representative of dynamical changes during weak geomagnetic disturbances, that is, outside of geomagnetic storms. The median Dst at zero epoch only reaches  $-18$  nT (cf., typical value of  $-9$  nT for all times). Only  $\sim 4.5\%$  of the epochs show evidence of storm conditions ( $\leq -50$  nT). As such our analysis is unlikely to be strongly influenced by adiabatic impacts (i.e., the “Dst-effect”; McIlwain, 1966).

### 3.2. SEA of MLT-Dependent >100-keV Electron Fluxes

Figure 1 is a reexamination of the SEA undertaken by Rodger et al. (2016), but presented in a MLT-dependent format and constrained to  $-1$  to  $+1$  days around the recurrent substorm zero epoch. Figure 1 uses the trapped >100-keV electron observations from the 90e2 channel. Many of the most interesting features seen in Figure 1 occur so quickly that they are not resolved in the  $-5$  to  $+15$  day format used in the earlier Rodger study, so we have limited the time axis to a much smaller range. Note that electrons drift around the Earth with increasing MLT, that is, from top to bottom. Figure 1 includes as a white line the empirical plasmapause location,  $L_{pp}$ , determined from the AE and MLT-dependent formulation given by O’Brien and Moldwin (2003).

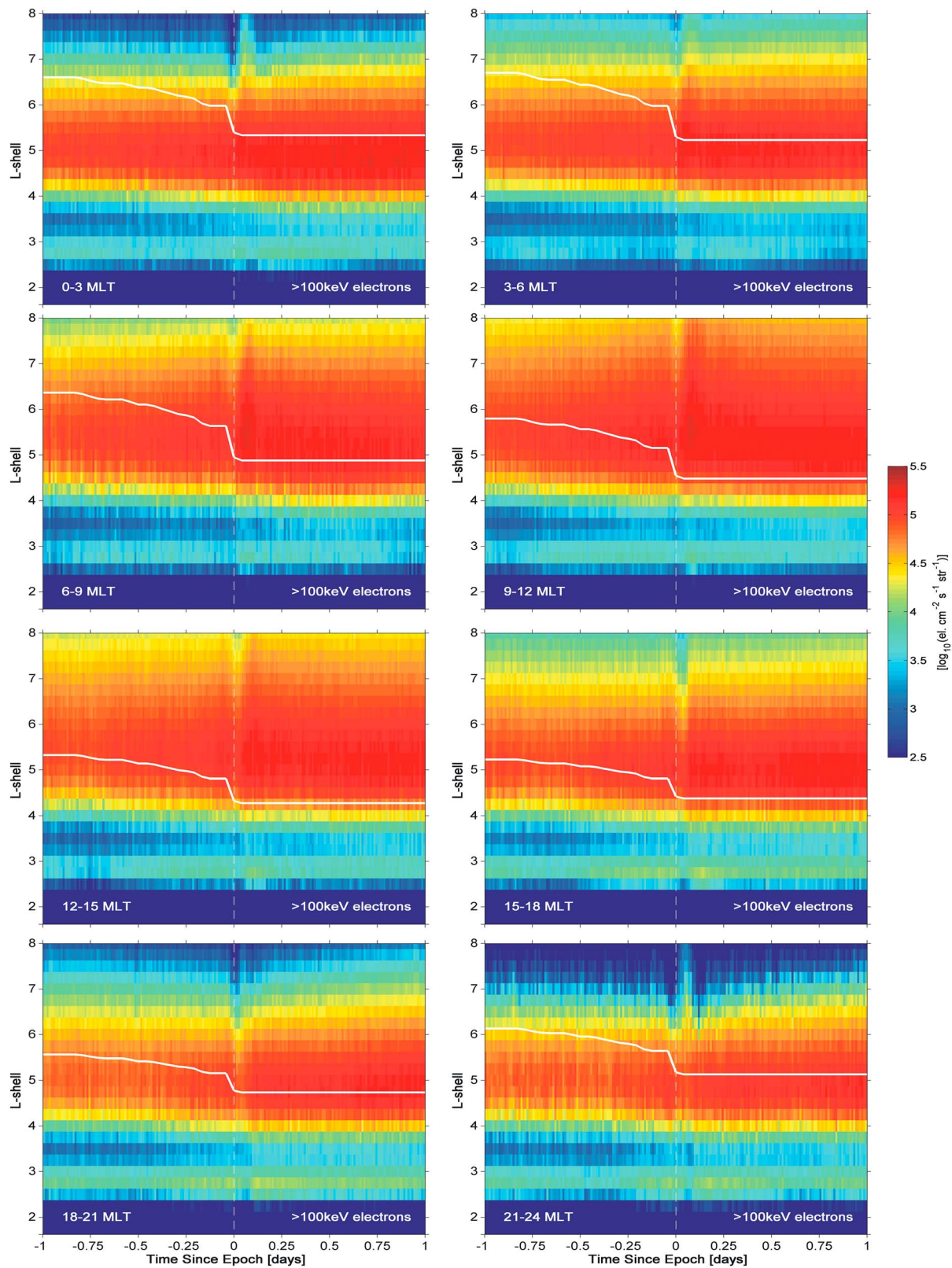


**Figure 1.** Superposed epoch analysis of median >100-keV Polar Orbiting Environmental Satellites (POES) trapped electrons for the Recurrent Substorm Epochs, plotted against  $L$ -shell. Each panel is for a different magnetic local time (MLT) range, as labeled. Plasmapause location is shown by the white line. Note that electrons drift around the Earth from top-left to bottom-right.

This figure demonstrates a number of strongly MLT-dependent features. From first principles, one expects magnetopause shadowing to start on the dayside, and substorm injections to occur on the nightside. Figure 1 is entirely consistent with those expectations. A sharp decrease in outer radiation belt flux occurs when  $L_{pp}$  moves sharply inward shortly before the zero epoch time. The sudden inward  $L_{pp}$  motion will go hand in hand with the inward motion of the magnetopause; both the inward motion of  $L_{pp}$  and the magnetopause result from the same dynamic changes in the solar wind. When the sudden dynamic pressure increase occurs in the solar wind, it brings with it an enhanced convection electric field due to the increase in solar wind velocity and/or IMF intensity. This electric field enhancement will result in the inward motion of the plasmopause as the balance between the magnetospheric convection and corotational electric fields readjusts. The driver of the corresponding decrease in flux at high  $L$ -shells is most likely a combination of magnetopause shadowing and outward transport.

In Figure 1 the dropout is very well defined in the 15–18 MLT range, more so than 12–15 MLT (or 9–12 MLT) where it likely begins. There is also a strong suggestion in the 15–18 MLT panel that the magnetopause shadowing begins at higher  $L$  and moves inward to lower  $L$ -shells. This is likely caused by a combination of the direct effect of magnetopause shadowing plus a cascade of losses to even lower  $L$ -shells (i.e., lower than those that are directly opened to the magnetopause after it moves inward). The lower  $L$ -shell loss cascade mentioned is likely due to very rapid outward radial transport that occurs after magnetopause shadowing; both can occur in tens of minutes to  $\sim 1$  hr (Shprits et al., 2006; Turner et al., 2012; Ukhorskiy et al., 2015).

At high  $L$ -shells Figure 1 shows evidence of a magnetopause shadowing-induced decrease occurring at all MLT before epoch time equal zero. This is possible as the dropout drifts around the Earth faster for higher  $L$ -shells (at  $L=7$  the drift period of a 150-keV electron is  $\sim 50$  min). It may also reflect a delay between the solar wind driver moving  $L_{pp}$  inward (signaling the starting of magnetopause shadowing at high  $L$ ), and the onset of the first substorm in the cluster which defines the epoch time. Substorms can be delayed relative to the responsible change in the solar wind on global-magnetospheric convective timescales.

Substorm produced electron injections are visible in Figure 1 across a wide range of large  $L$ -shells on the nightside. These are seen as new sharp increases starting in the 21–24 and 0–3 MLT panels. It is these injections, and subsequent processes triggered by those injections, which replace the electrons lost from the dropout event, and indeed, they lead to an additional enhancement. We suggest that this is consistent with the importance of substorm injections, rather than large-scale convection, in outer belt electron acceleration, supporting the conclusions of Jaynes et al. (2015) and Rodger et al. (2016). Figure 1 demonstrates the importance of considering the interaction of MLT-dependent processes when considering radiation belt dynamical processes.

The dropouts observed by POES penetrate to low  $L$ -shells, with discernible effects down to  $L \sim 4$ , although that feature becomes less and less obvious at those lower  $L$ -shells in the statistical picture presented here. There is an ongoing debate concerning the mechanism responsible for such dropouts. Some models (e.g., Mann et al., 2016; Ukhorskiy et al., 2015) indicate that magnetopause shadowing and outward radial transport are sufficient to cause electron dropouts down to  $L = 4$ , while others (e.g., Shprits, 2013) conclude that some additional loss mechanism is necessary for dropouts to extend down to such low  $L$ -shells. In that latter case electromagnetic ion cyclotron waves causing precipitation into the atmosphere are invoked as the most likely candidate. In reality, both processes are likely important and contribute differently on a case-by-case basis. Considering that perspective, it is important to look for telltale signatures of both loss processes using guidelines established by previous studies (e.g., Aseev et al., 2017; Shprits et al., 2017; Turner et al., 2014; Xiang et al., 2017).

### 3.3. SEA of MLT-Dependent 52-keV Proton Fluxes

We follow the same processes and undertake SEA on the 52-keV trapped proton observations (from the 90P1 channel). The proton SEA allows us to test a number of predictions where behavior should be charge dependent or independent. This SEA is shown in Figure 2, in the same format as Figure 1. Protons will drift in the opposite direction to electrons, that is, from high to low MLT, or bottom to top in Figure 2.

A number of features are shared between Figures 1 and 2. Magnetopause shadowing is clearly defined for MLTs near the dayside, although we argue that it evolves in the opposite way to that seen in Figure 1, that is, starting from 12 to 15 MLT to be very clear in the 9–12 and 6–9 MLT panels. This is consistent with the

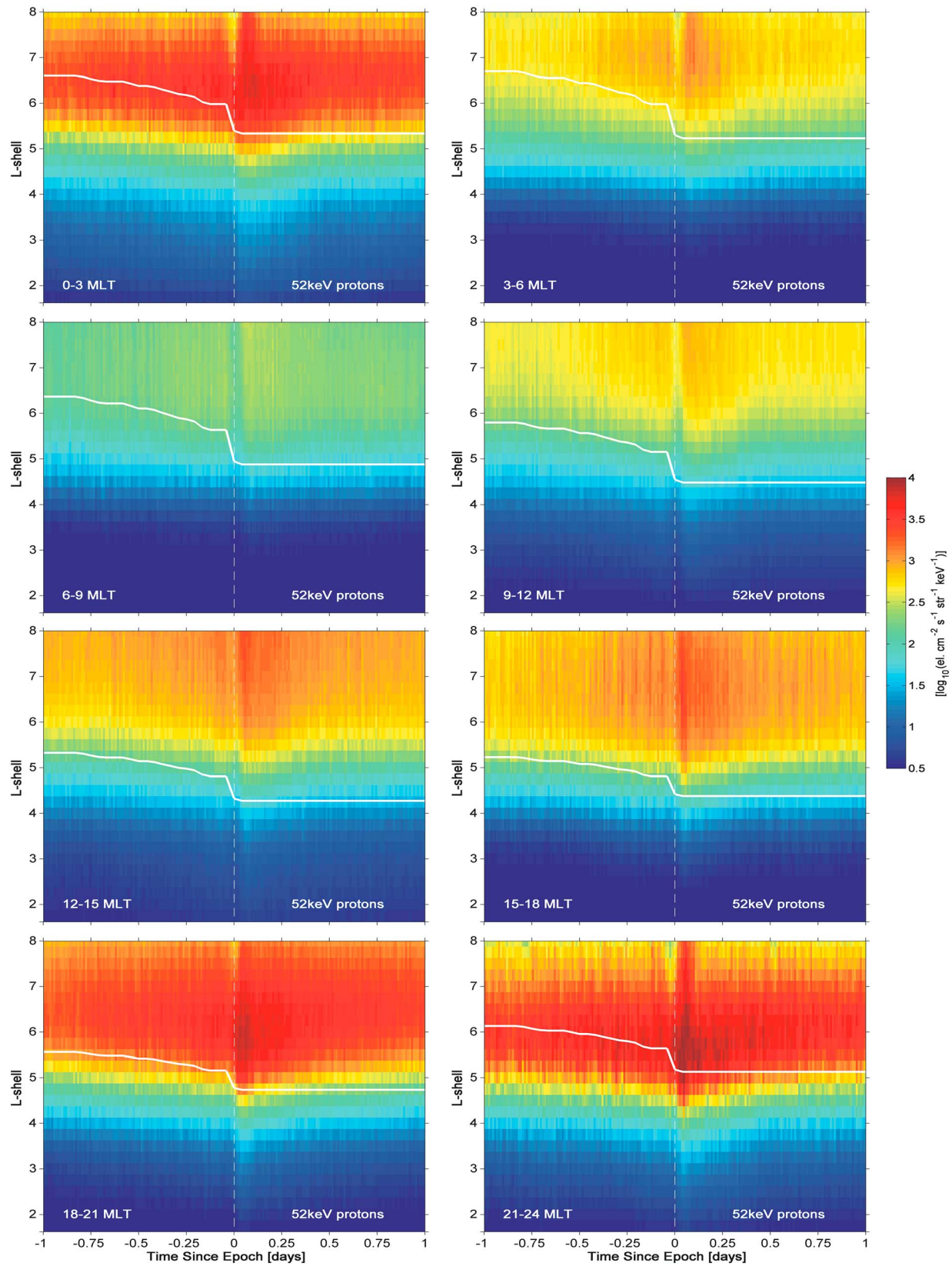


**Figure 2.** As for Figure 1, but now showing the superposed epoch analysis for 52 keV protons. Note that protons drift around the Earth from bottom-right to top-left.

direction of proton drift. The magnetopause shadowing starts at the time of a sharp decrease in  $L_{pp}$ , as was seen for the electrons. Magnetopause shadowing is expected to be independent of particle charge, mass, or energy, such that electrons or protons, which are drifting around the Earth on the same  $L$ -shell (but in opposite directions), will encounter the magnetopause and hence be lost. The timing of the dropout signature is very similar in both Figures 1 and 2, consistent with charge independence and hence the magnetopause shadowing loss process—rather than, for example, wave particle interactions.

The dynamics of protons in this energy range are less complex than those for electrons; for example, there are no significant wave-particle interactions driving acceleration, so the proton buildup is likely due to injections from the tail. This may be why the magnetopause shadowing signature is so clear and sharp in Figure 2. The figure seems to show that on the dayside, the dropout stretches from high  $L$  inward to at least  $L=4$ , where the proton flux becomes insignificant. This is clearest in the panels for 9–12 and 6–9 MLT. In contrast, for 3–6 or 0–3 MLT the dropout appears to start earlier at higher  $L$  and start later at lower  $L$ ; likely due to faster drift times for higher  $L$ .

Figure 2 also shows increases in protons fluxes just after the zero epoch, consistent with simultaneous substorm-linked enhancements of protons and electrons. These are most clear in the nightside panels (03 and 21–24 MLT). The proton enhancements are clearly present down to very low  $L$ -shells, at least  $L=2.25$ . We believe that these are much lower  $L$ -shells than would be generally expected for a substorm injection event, and note that the SEA median fluxes at these  $L$ -shells are very low. The enhancements then progressively drift around the Earth, with the injection arriving later on the morning side. As in the case for electrons, the substorm-linked enhancements “refill” the magnetopause shadowing-produced dropout. One strong feature present in Figure 2 is the low proton fluxes seen for all times in the 6–9 MLT region. This might be indicative of the “null” or “turning point” of protons’ drift trajectories. Looking at the dawn quadrant outside of the Alfvén layer, protons drift trajectories will execute a sharp turnaround in this MLT region (e.g., Kivelson and Russell, Fig 10.25, 1995). We suggest that this will result in the observed void on the dayward side of that null region possibly due to interactions on the dayside near the magnetopause.

The consistency of Figures 1 and 2 in terms of timing, charge dependent drift directions, and charge independent dropouts are strong demonstrations of magnetopause shadowing produced losses, and the ability of substorms to directly compensate for those losses in these energy ranges.

#### 4. Consequences for SPELLS Events

During even mildly geomagnetically disturbed periods, electrons ranging in energy from tens of keV up to ~1 MeV can be quickly (in a few hours or less) injected into the slot and inner radiation belt ( $L<3$ ) in events termed SPELLS (Turner et al., 2017). Evidence has been shown that the injections may serve as the dominant source of tens to hundreds of keV electrons in Earth’s inner radiation belt. The physical mechanism responsible for these events is to date, unclear.

One suggested SPELLS-production mechanism (Lejosne et al., 2018) is due to subauroral polarization streams (SAPSs), which cause localized potential drops in the premidnight region. The mechanism relies on SAPS-produced electric fields helping energetic electrons to deeply penetrate the inner magnetosphere. A prediction of this mechanism is that the energetic electrons will penetrate more deeply than the energetic ions, due to their differing charge.

It has long been recognized that the POES MEPED instruments are not particularly sensitive to energetic electrons (Rodger, Clilverd, et al., 2010; Yando et al., 2011), especially in comparison with those instruments onboard the Van Allen Probes. It is clear, however, that the POES data can detect the inner belt >100-keV electron enhancement, which occurs during the mildly geomagnetically disturbed times around recurrent substorm epochs (as seen in Figure 4 of Rodger et al., 2016). At the times of recurrent substorm epochs relatively low energy (52keV) protons are injected to  $L$ -shells equivalent to the inner radiation belt, but only for relatively short time periods (hours), after which their fluxes drop to the noise floor. The time period of hours is consistent with losses due to charge exchange at lower  $L$ -shells.

One might argue that this proton injection is inconsistent with the SAPSs mechanism. However, it seems important to know that the proton injection is fairly sharp and only occurs shortly after the start of the recurrent substorm epochs. In contrast, the inner radiation belt and slot region electron enhancements are not as

sharply defined as the proton and outer radiation belt electron injections are. It is not totally clear that these observations rule out the SAPS argument, but neither do they support that suggestion.

We have argued that the recurrent substorm processes and SPELLS are likely to be linked. Both occur during mildly disturbed geomagnetic conditions and involve electron enhancements at very low  $L$ -shells. To further investigate this, we undertook SEA using the times of RBSP-observed SPELLS events as the epochs. SPELLS epochs were defined as the first observation time of a sudden enhancement in electron flux in the slot and inner zone by Van Allen Probes, which should bound the actual time of the SPELLS to within 4.5 hr or less. There were 143 such epochs, spanning the time range from 2 December 2012 to 20 November 2014. Figure 3a shows the SEA using these SPELLS epochs undertaken on the daily number of SuperMAG-reported substorms (Newell, Gjerloev, 2011b). The blue line shows the daily variation in daily substorm number, while the two black lines show the upper and lower quartiles. During the period from the start of 2012 to the end of 2014, the median number of substorms per day was 2. In contrast, on the day of the SPELLS zero epoch, the median substorm number is 5 (ranging from 3 to 7 across the quartiles). This is consistent with strong substorm activity occurring in the same time period as SPELLS, and potentially providing the energy for the SPELLS mechanism.

Finally, we show that the solar wind drivers and geomagnetic conditions around recurrent substorm epochs and SPELLS epochs are very similar. We independently undertook SEA for both sets of epochs, producing Figure 3b. The four left-hand panels are the SEA for the 143 SPELLS-epochs, while the four right-hand panels are those for the 2,052 recurrent substorm epochs. In all cases 1-hr time resolution is used. From top to bottom, Figure 3 shows the solar wind pressure, solar wind Epsilon parameter (Akasofu, 1981), SEA for IMF  $B_z$ , and the SuperMAG-determined AU equivalent (often termed SMU). Note that the three solar wind parameters were shifted to the Earth's bow shock nose.

As the left-hand panels involve  $\sim 14$  times fewer epochs than the right hand panels, the SEA are much noisier than those shown for the recurrent substorm epochs. However, we argue that there is close agreement in the two sets of SEA, with variations occurring on similar time scales and with very similar magnitudes. As such it seems likely that SPELLS events are likely a subset of the recurrent SS events. It is telling that 78% of the SPELLS events can be linked to recurrent substorms. As such, the low- $L$  electron enhancements should be fairly common during recurrent substorms, consistent with the SEA shown in Figure 4 of Rodger et al. (2016).

## 5. Summary and Discussion

In this study we have examined dynamical variations in the radiation belt during times of mild geomagnetic disturbance. It is not uncommon for researchers to focus on strong storms to consider changes in the radiation belts; our results demonstrate that very mild disturbances are also associated with multiple processes leading to loss and enhancements in flux. These changes are not limited to the outer belts but extend even into the inner belt and slot region. We have focused on time periods with high solar wind speeds where clusters of substorms occur. Around these times convection from the solar wind and fresh particle injections from the substorms are both present, likely leading to enhanced plasma wave activity. Our results demonstrate clear signatures of magnetopause shadowing impacting both electrons and protons. We have also shown how dayside magnetopause shadowing losses interact with nightside substorm-produced enhancements, leading to consistent MLT-dependent patterns.

We have shown that SPELLS events occur during the same conditions as periods of recurrent (or clustered) substorms, and that it is likely that the low- $L$  electron flux enhancements are somehow linked to the substorms. Recurrent substorm epochs have been shown to display SPELLS-like enhancements. However, the enhancements are not sharply onset around the substorm cluster start, and it is certainly not clear that the SPELLS electron enhancement is directly linked to the start of the recurrent substorm cluster. Rather, these seem to be geophysically linked. This would be consistent with SAPS as a production mechanism, as these are correlated with substorms.

As noted earlier, much recent progress has been provided by large, very high quality, but high cost, flagship missions; such spacecraft cannot, unfortunately, provide much simultaneous MLT and  $L$  coverage. However, we are now at the start of a revolution in low cost access to space, alongside the development of

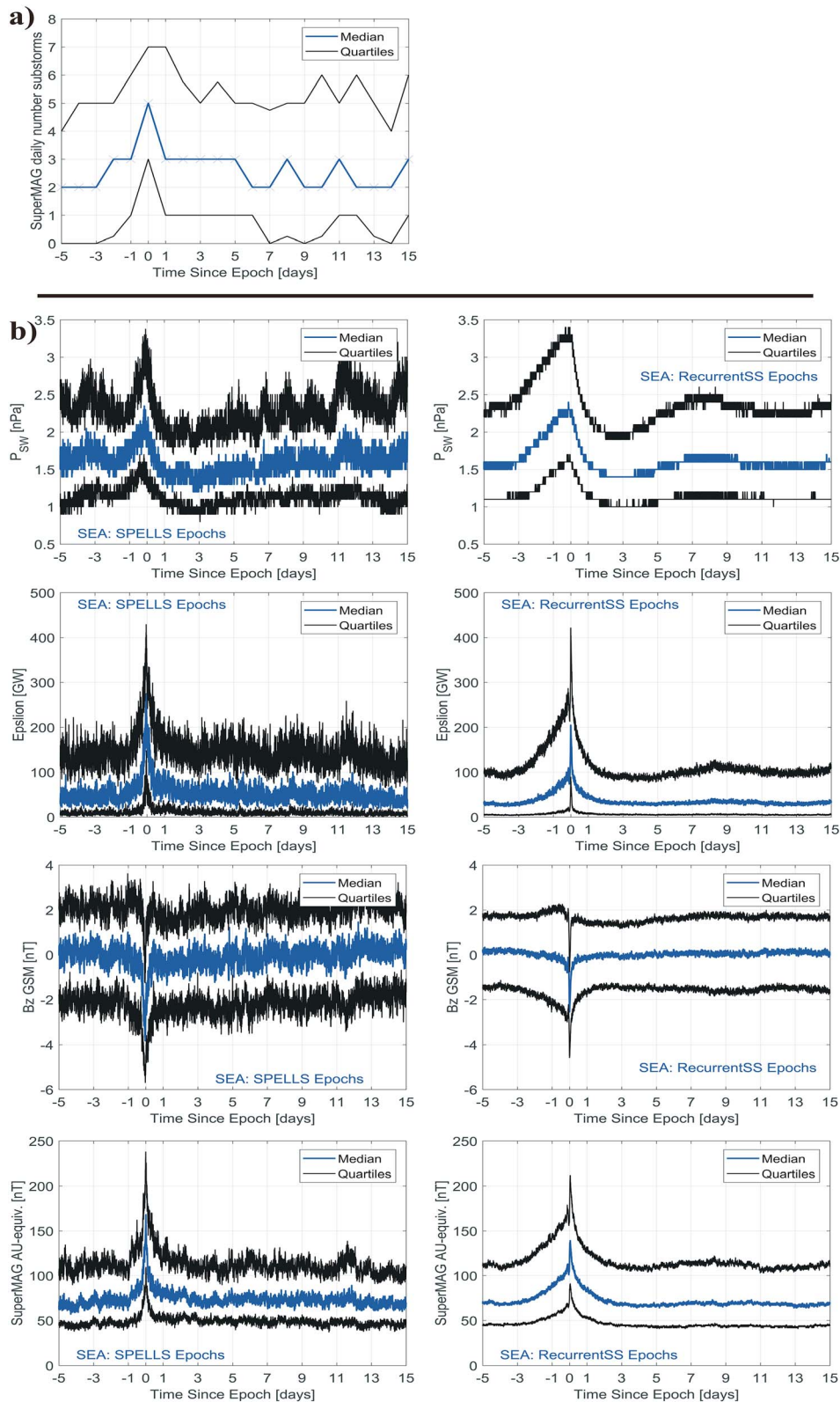


**Figure 3.** Upper panel (a): Superposed epoch analysis of the number of SuperMAG reported substorms per day for the Van Allen Probes-observed sudden particle enhancements at low  $L$  shells (SPELLS) epochs. The blue line is the median, while the black lines are the upper and lower quartiles. Lower panels (b): Superposed epoch analysis of the number of solar wind and SuperMAG reported AU index for the Van Allen Probes-observed SPELLS epochs (lower four left-hand panels) and the recurrent substorm epochs (lower four right-hand panels).

relatively low mass, low power, but very high quality radiation belt experiments. Some examples are Colorado/Laboratory for Atmospheric and Space Physics' Colorado Student Space Weather Experiment (CSSWE), AeroCube-6, University of New Hampshire/MontanaState's FIREBIRD, and University of California, Los Angeles' ELFEN, AlbertaSat. New instruments are becoming available that are suitable for deployment on cubesats—opening up the possibility of large constellations to truly image the rapid dynamics of radiation belts processes. Such CubeSat missions are not limited to LEO, with examples of radiation belt CubeSat's planned for geostationary transfer orbit (e.g., GTOSat (Blum et al., 2018)). We suggest that this study shows the value of simultaneous multiplatform observations allowing MLT and *L*-coverage, even if with limited instrumentation.

#### Acknowledgments

The authors would like to thank the researchers and engineers of NOAA's Space Environment Center for the provision of the data and the operation of the SEM-2 instrument carried onboard these spacecraft. For the substorm list we gratefully acknowledge the SuperMAG initiative and the SuperMAG collaborators. M. A. C. acknowledges funding support from the Natural Environment Research Council Highlight Topic grant NE/P10738X/1 (Rad-Sat). Data availability is described at the following websites: <https://www.ngdc.noaa.gov/stp/satellite/poes/dataaccess.html> (POES SEM observations), <http://supermag.jhuapl.edu/substorms/> (SuperMAG substorms), and <http://supermag.jhuapl.edu/indices/> (magnetic indices and solar wind parameters from SuperMAG). Van Allen Probes data are freely available on the science gateway site: <http://rbspgway.jhuapl.edu/>.

#### References

- Akasofu, S. I. (1981). Energy coupling between the solar wind and the magnetosphere. *Space Science Reviews*, 28(2), 121–190. <https://doi.org/10.1007/BF00218810>
- Aseev, N. A., Shprits, Y. Y., Drozdov, A. Y., Kellerman, A. C., Usanova, M. E., Wang, D., & Zhelavskaya, I. S. (2017). Signatures of ultra-relativistic electron loss in the heart of the outer radiation belt measured by Van Allen Probes. *Journal of Geophysical Research: Space Physics*, 122, 10,102–10,111. <https://doi.org/10.1002/2017JA024485>
- Baker, D. N. P., Erickson, J., Fennell, J. F., Foster, J. C., Jaynes, A. N., & Verronen, P. T. (2018). Space weather effects in the Earth's radiation belts. *Space Science Reviews*, 214(1). <https://doi.org/10.1007/s11214-017-0452-7>
- Balasis, G. I., Daglis, A., & Mann, I. R. (2016). *Waves, particles, and storms in Geospace: A complex interplay*. Oxford: Oxford Univ Press. ISBN-13: 9780198705246
- Blum, L., K. Shrikanth, X. Li, L. Kepko, A. Jones, Q. Schiller (2018). CubeSat missions to study radiation belt electron dynamics and loss, 42nd COSPAR Scientific Assembly, 2018cosp...42E.383B
- Carson, B. R., Rodger, C. J., & Clilverd, M. A. (2012). POES satellite observations of EMIC-wave driven relativistic electron precipitation during 1998–2010. *Journal of Geophysical Research Space Physics*, 118, A02313. <https://doi.org/10.1029/2012JA017998>
- Cresswell-Moorcock, K., Rodger, C. J., Kero, A., Collier, A. B., Clilverd, M. A., Häggström, I., & Pitkänen, T. (2013). A reexamination of latitudinal limits of substorm-produced energetic electron precipitation. *Journal of Geophysical Research: Space Physics*, 118, 6694–6705. <https://doi.org/10.1002/jgra.50598>
- Douma, E., Rodger, C. J., Blum, L. W., & Clilverd, M. A. (2017). Occurrence characteristics of relativistic electron microbursts from SAMPEX observations. *Journal of Geophysical Research: Space Physics*, 122, 8096–8107. <https://doi.org/10.1002/2017JA024067>
- Evans, D. S., & M. S. Greer (2004). Polar Orbiting Environmental Satellite Space Environment Monitor-2 instrument descriptions and archive data documentation, NOAA technical Memorandum version 1.4, Space Environment Laboratory, Colorado.
- Gjerloev, J. W. (2012). The SuperMAG data processing technique. *Journal of Geophysical Research*, 117(A9), A09213. <https://doi.org/10.1029/2012JA017683>
- Henry, A. T., Rodger, C. J., Clilverd, M. A., Engebretson, M. J., Mann, I. R., Lessard, M. R., et al. (2016). Confirmation of EMIC wave-driven relativistic electron precipitation. *Journal of Geophysical Research: Space Physics*, 121, 5366–5383. <https://doi.org/10.1002/2015JA022224>
- Jaynes, A. N., Baker, D. N., Singer, H. J., Rodriguez, J. V., Loto'aniu, T. M., Ali, A. F., et al. (2015). Source and seed populations for relativistic electrons: Their roles in radiation belt changes. *Journal of Geophysical Research: Space Physics*, 120, 7240–7254. <https://doi.org/10.1002/2015JA021234>
- Kasahara, S., Miyoshi, Y., Yokota, S., Mitani, T., Kasahara, Y., Matsuda, S., et al. (2018). Pulsating aurora from electron scattering by chorus waves. *Nature*, 554(7692), 337–340. <https://doi.org/10.1038/nature25505>
- Kivelson, M. G., & Russell, C. T. (Eds) (1995). *Introduction to space physics*. New York: Cambridge University Press.
- Lejosne, S., Kunduri, B. S. R., Mozer, F. S., & Turner, D. L. (2018). Energetic electron injections deep into the inner magnetosphere: A result of the subauroral polarization stream (SAPS) potential drop. *Geophysical Research Letters*, 45(9), 3811–3819. <https://doi.org/10.1029/2018GL077969>
- Lyons, L. R., Lee, D.-Y., Thorne, R. M., Horne, R. B., & Smith, A. J. (2005). Solar wind-magnetosphere coupling leading to relativistic electron energization during high-speed streams. *Journal of Geophysical Research*, 110(A11), A11202. <https://doi.org/10.1029/2005JA011254>
- Mann, I. R., Ozeke, L. G., Murphy, K. R., Claudepierre, S. G., Turner, D. L., Baker, D. N., et al. (2016). Explaining the dynamics of the ultra-relativistic third Van Allen radiation belt. *Nature Physics*, 12(10), 978–983. <https://doi.org/10.1038/NPHYS3799>
- McIlwain, C. E. (1966). Ring current effects on trapped particles. *Journal of Geophysical Research*, 71(15), 3623–3628. <https://doi.org/10.1029/JZ071i015p03623>
- Miyoshi, Y., Kataoka, R., Kasahara, Y., Kumamoto, A., Nagai, T., & Thomsen, M. F. (2013). High-speed solar wind with southward interplanetary magnetic field causes relativistic electron flux enhancement of the outer radiation belt via enhanced condition of whistler waves. *Geophysical Research Letters*, 40, 4520–4525. <https://doi.org/10.1002/grl.50916>
- Newell, P. T., & Gjerloev, J. W. (2011a). Evaluation of SuperMAG auroral electrojet indices as indicators of substorms and auroral power. *Journal of Geophysical Research*, 116(A12), A12211. <https://doi.org/10.1029/2011JA016779>
- Newell, P. T., & Gjerloev, J. W. (2011b). Substorm and magnetosphere characteristic scales inferred from the SuperMAG auroral electrojet indices. *Journal of Geophysical Research*, 116(A12), A12232. <https://doi.org/10.1029/2011JA016936>
- O'Brien, T. P., & Moldwin, M. B. (2003). Empirical plasmopause models from magnetic indices. *Geophysical Research Letters*, 30(4), 1152. <https://doi.org/10.1029/2002GL016007>
- Rodger, C. J., Carson, B. R., Cummer, S. A., Gamble, R. J., Clilverd, M. A., Green, J. C., et al. (2010). Contrasting the efficiency of radiation belt losses caused by ducted and nonducted whistler-mode waves from ground-based transmitters. *Journal of Geophysical Research*, 115(A12), A12208. <https://doi.org/10.1029/2010JA015880>
- Rodger, C. J., Clilverd, M. A., Green, J. C., & Lam, M. M. (2010). Use of POES SEM-2 observations to examine radiation belt dynamics and energetic electron precipitation into the atmosphere. *Journal of Geophysical Research*, 115(A4), A04202. <https://doi.org/10.1029/2008JA014023>

- Rodger, C. J., Cresswell-Moorcock, K., & Clilverd, M. A. (2016). Nature's Grand Experiment: Linkage between magnetospheric convection and the radiation belts. *Journal of Geophysical Research: Space Physics*, *121*, 171–189. <https://doi.org/10.1002/2015JA021537>
- Shprits, Y. Y. (2013). Unusual stable trapping of the ultrarelativistic electrons in the Van Allen radiation belts. *Nature Physics*, *9*, 699–703. <https://doi.org/10.1038/NPHYS2760>
- Shprits, Y. Y., Kellerman, A., Aseev, N., Drozdov, A. Y., & Michaelis, I. (2017). Multi-MeV electron loss in the heart of the radiation belts. *Geophysical Research Letters*, *44*, 1204–1209. <https://doi.org/10.1002/2016GL072258>
- Shprits, Y. Y., Thorne, R. M., Horne, R. B., & Summers, D. (2006). Bounce-averaged diffusion coefficients for field-aligned chorus waves. *Journal of Geophysical Research*, *111*(A10), A10225. <https://doi.org/10.1029/2006JA011725>
- Simms, L., Engebretson, M., Clilverd, M., Rodger, C., Lessard, M., Gjerloev, J., & Reeves, G. (2018). A distributed lag autoregressive model of geostationary relativistic electron fluxes: Comparing the influences of waves, seed and source electrons, and solar wind inputs. *Journal of Geophysical Research: Space Physics*, *123*(5), 3646–3671. <https://doi.org/10.1029/2017JA025002>
- Summers, D., Thorne, R. M., & Xiao, F. (1998). Relativistic theory of wave-particle resonant diffusion with application to electron acceleration in the magnetosphere. *Journal of Geophysical Research*, *103*(A9), 20,487–20,500. <https://doi.org/10.1029/98JA01740>
- Turner, D. L., Angelopoulos, V., Morley, S. K., Henderson, M. G., Reeves, G. D., Li, W., et al. (2014). On the cause and extent of outer radiation belt losses during the 30 September 2012 dropout event. *Journal of Geophysical Research: Space Physics*, *119*, 1530–1540. <https://doi.org/10.1002/2013JA019446>
- Turner, D. L., Kilpua, E. K. J., Hietala, H., Claudepierre, S. G., O'Brien, T. P., Fennell, J. F., et al. (2019). The response of Earth's electron radiation belts to geomagnetic storms: Statistics from the Van Allen Probes era including effects from different storm drivers. *Journal of Geophysical Research: Space Physics*, *124*(2), 1013–1034. <https://doi.org/10.1029/2018JA026066>
- Turner, D. L., O'Brien, T. P., Fennell, J. F., Claudepierre, S. G., Blake, J. B., Jaynes, A. N., et al. (2017). Investigating the source of near-relativistic and relativistic electrons in Earth's inner radiation belt. *Journal of Geophysical Research: Space Physics*, *122*, 695–710. <https://doi.org/10.1002/2016JA023600>
- Turner, D. L., Shprits, Y., Hartinger, M., & Angelopoulos, V. (2012). Explaining sudden losses of outer radiation belt electrons during geomagnetic storms. *Nature Physics*, *8*(3), 208–212. <http://doi.org/10.1038/nphys2185>
- Ukhorskiy, A. Y., Sitnov, M. I., Millan, R. M., Kress, B. T., Fennell, J. F., Claudepierre, S. G., & Barnes, R. J. (2015). Global storm time depletion of the outer electron belt. *Journal of Geophysical Research: Space Physics*, *120*, 2543–2556. <https://doi.org/10.1002/2014JA020645>
- van de Kamp, M., Rodger, C. J., Seppälä, A., Clilverd, M. A., & Verronen, P. T. (2018). An updated model providing long-term data sets of energetic electron precipitation, including zonal dependence. *Journal of Geophysical Research: Atmospheres*, *123*(17), 9891–9915. <https://doi.org/10.1029/2017JD028253>
- Walt, M. (1994). *Introduction to geomagnetically trapped radiation*. Cambridge: Cambridge University Press. <https://doi.org/10.1017/CBO9780511524981>
- Xiang, Z., Tu, W., Li, X., Ni, B., Morley, S. K., & Baker, D. N. (2017). Understanding the mechanisms of radiation belt dropouts observed by Van Allen Probes. *Journal of Geophysical Research: Space Physics*, *122*, 9858–9879. <https://doi.org/10.1002/2017JA024487>
- Xiang, Z., Tu, W., Ni, B., Henderson, M. G., & Cao, X. (2018). A statistical survey of radiation belt dropouts observed by Van Allen Probes. *Geophysical Research Letters*, *45*(16), 8035–8043. <https://doi.org/10.1029/2018GL078907>
- Yando, K., Millan, R. M., Green, J. C., & Evans, D. S. (2011). A Monte Carlo simulation of the NOAA POES Medium Energy Proton and Electron Detector instrument. *Journal of Geophysical Research*, *116*(A10), A10231. <https://doi.org/10.1029/2011JA016671>
- Yu, Y., Koller, J., & Morley, S. K. (2013). Quantifying the effect of magnetopause shadowing on electron radiation belt dropouts. *Annales de Geophysique*, *31*(11), 1929–1939. <https://doi.org/10.5194/angeo-31-1929-2013>
- Zhao, H., Baker, D. N., Jaynes, A. N., Li, X., Elkington, S. R., Kanekal, S. G., et al. (2017). On the relation between radiation belt electrons and solar wind parameters/geomagnetic indices: Dependence on the first adiabatic invariant and  $L^*$ . *Journal of Geophysical Research: Space Physics*, *122*, 1624–1642. <https://doi.org/10.1002/2016JA023658>